

Exotic phase diagram of a topological quantum system

Xiao-Feng Shi, Yan Chen, and J. Q. You

Department of Physics and State Key Laboratory of Surface Physics, Fudan University, Shanghai 200433, China

(Dated: December 2, 2018)

We study the quantum phase transitions (QPTs) in the Kitaev spin model on a triangle-honeycomb lattice. In addition to the ordinary topological QPTs between Abelian and non-Abelian phases, we find new QPTs which can occur between two phases belonging to the same topological class, namely, either two non-Abelian phases with the same Chern number or two Abelian phases with the same Chern number. Such QPTs result from the singular behaviors of the nonlocal spin-spin correlation functions at the critical points.

I. INTRODUCTION

A quantum phase transition (QPT) involves an abrupt change of the ground state in a many-body system due to its quantum fluctuations.¹ Discovering and characterizing new QPTs in a two-dimensional topological quantum system have recently attracted considerable interest.^{2–5} Because the ground states in some topological quantum systems (e.g., the Kitaev spin models on honeycomb³ and triangle-honeycomb⁵ lattices) are exactly solvable, QPTs in these systems can be analytically investigated. In these topological systems, the discovered QPTs include the transition between a gapped Abelian phase and a gapless phase,^{4,6} the transition between Abelian and non-Abelian phases,^{5,7–10} and the transition between two non-Abelian phases with different Chern numbers.³ Also, an unconventional QPT between two non-Abelian phases was found¹¹ in the Kitaev spin model on a triangle-honeycomb lattice by a fermionization method. Nevertheless, to the best of our knowledge, the QPT between two topological phases of the same Chern number (which belong to the same topological class) has not yet been found.

Here we show that, in the Kitaev spin model on a triangle-honeycomb lattice, a QPT can indeed happen between two gapped phases in the same topological class, in addition to the ordinary topological QPT between two phases of different Chern numbers. To demonstrate this, we focus on two parameter regimes as typical examples: (i) When the parameters vary across a critical curve separating two gapped phases of the same Chern number $\nu = 0$ or ± 1 , a first-order QPT occurs; (ii) when the parameters vary across a special critical point where several critical curves meet, a continuous QPT can occur. This is due to the exotic ground-state phase diagram which has *either* critical curves between two gapped phases (with the same or different Chern numbers) *or* critical points where four different gapped phases (with Chern numbers 0, 0, 1 and -1) terminate. These results reveal that the Kitaev spin model on a triangle-honeycomb lattice exhibits novel topological properties. Moreover, we find that such QPTs result from the singular behaviors of the nonlocal spin-spin correlations at the critical points.

The paper is organized as follows. In Sec. II, we present the solution for the ground state of the Hamiltonian in

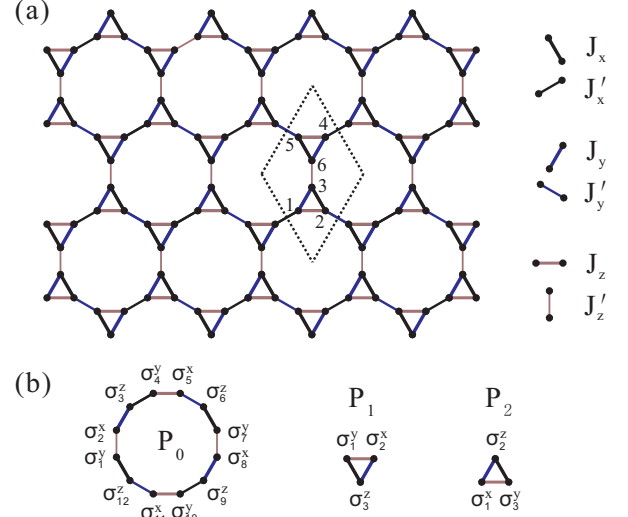


FIG. 1: (Color online) (a) A schematic illustration of the Kitaev spin model on a triangle-honeycomb lattice. Each unit cell (dotted diamond) contains six spins at sites 1,2,...,6. The six types of bonds are labeled by J_α and J'_α , where $\alpha = x, y, z$. (b) Schematic diagrams of the three plaquette operators P_0 , P_1 , and P_2 , which are defined in Eq. (2).

the uniform-flux sector. Sections III and IV show two typical phase diagrams of the ground-state wavefunctions and study various QPTs in the considered Kitaev spin model. Finally, a brief conclusion is given in Sec. V.

II. GROUND STATE IN THE UNIFORM-FLUX SECTOR

The Kitaev spin model on a triangle-honeycomb lattice is schematically shown in Fig. 1(a) and the model Hamiltonian is given by

$$\begin{aligned}
 H = & J_x \sum_{x\text{-link}} \sigma_i^x \sigma_j^x + J_y \sum_{y\text{-link}} \sigma_i^y \sigma_j^y + J_z \sum_{z\text{-link}} \sigma_i^z \sigma_j^z \\
 & + J'_x \sum_{x'\text{-link}} \sigma_i^x \sigma_j^x + J'_y \sum_{y'\text{-link}} \sigma_i^y \sigma_j^y + J'_z \sum_{z'\text{-link}} \sigma_i^z \sigma_j^z,
 \end{aligned} \tag{1}$$

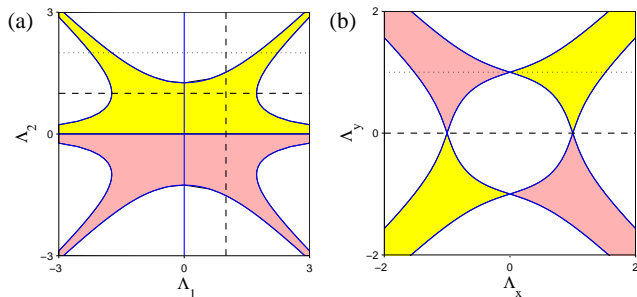


FIG. 2: (Color online) The ground-state phase diagram of the Kitaev spin model on a triangle-honeycomb lattice. (a) $\Lambda_1 = J'_x/J_x$, and $\Lambda_2 = J_z/J_x$, when $J_x = J_y$, $J'_x = J'_y$, and $J_z J'_x = J'_z J_x$. (b) $\Lambda_x = J_x/J_z$, and $\Lambda_y = J_y/J_z$, when $J_x = J'_x$, $J_y = J'_y$, and $J_z = J'_z$. The solid curves or lines correspond to gapless phases. The yellow (red) regions in (a) and (b) correspond to gapped phases with Chern number $\nu = 1$ (-1). The white regions are gapped phases with Chern number $\nu = 0$.

where σ_i^α , with $\alpha = x, y$ and z , are the three Pauli operators at site i . Among the six sums in Eq. (1), four involve interactions within each unit cell (see Fig. 1): (i) The x -link couples either spins 2 and 3 or spins 5 and 6, (ii) the y -link couples either spins 1 and 3 or spins 4 and 6, (iii) the z -link couples either spins 1 and 2 or spins 4 and 5, and (iv) the z' -link couples spins 3 and 6. Nearest-neighbor unit cells are coupled by the x' - and y' -links. As found in Ref. 5, the ground state of Hamiltonian (1) is at least 8 (6)-fold degenerate for the Abelian (non-Abelian) phase.

For the three types of hermitian plaquette operators defined by [see Fig. 1(b)]

$$\begin{aligned} P_0 &\equiv \sigma_1^y \sigma_2^x \sigma_3^z \sigma_4^y \sigma_5^x \sigma_6^z \sigma_7^y \sigma_8^x \sigma_9^z \sigma_{10}^y \sigma_{11}^x \sigma_{12}^z, \\ P_1 &\equiv \sigma_1^y \sigma_2^x \sigma_3^z, \quad P_2 \equiv \sigma_1^x \sigma_2^z \sigma_3^y, \end{aligned} \quad (2)$$

each has eigenvalues ± 1 . These plaquette operators commute with not only each other but also the Hamiltonian (1). As verified in Ref. 5, the ground state of Hamiltonian (1) is *either* in the sector of the Hilbert space in which all plaquette operators in Eq. (2) have eigenvalue one *or* in the sector where the time-reversal transformation of each plaquette operator in Eq. (2) has eigenvalue one. The former is denoted as the uniform-flux sector.¹²

By using the Jordan-Wigner transformation, Hamiltonian (1) can be converted to a form represented by Majorana fermions.⁵ Performing Fourier transform on the Hamiltonian in the uniform-flux sector, we obtain

$$H_u = \sum_{\mathbf{k} \in \text{BZ}, j=1}^3 \varepsilon_{\mathbf{k}}^{(j)} \left[2A_{\mathbf{k}}^{(j)\dagger} A_{\mathbf{k}}^{(j)} - 1 \right], \quad (3)$$

where BZ denotes the first Brillouin zone. In Eq. (3), $A_{\mathbf{k}}^{(j)\dagger} = \sum_{s=1}^6 c_{\mathbf{k}}^{(s)} w_s$ are fermionic operators, where $c_{\mathbf{k}}^{(s)}$ is the Fourier transform of the Majorana fermionic operator at site s ($s = 1, 2, \dots, 6$) in a unit cell, and w_s

is a function of variable $\varepsilon_{\mathbf{k}}^{(j)}$ (see Appendix A). One can prove that Hamiltonian (3) breaks time reversal symmetry from the property of Majorana fermions $c_{\mathbf{k}}^{(s)}$. This is in sharp contrast to the Kitaev model on a honeycomb lattice in which the time reversal symmetry is preserved. This is due to the difference between the bipartite nature of the honeycomb lattice and the non-bipartite nature of the triangle-honeycomb lattice. Hamiltonian (3) has six energy bands: $\varepsilon_{\mathbf{k}}^{(1)} = -\varepsilon_{\mathbf{k}}^{(6)} = -\varepsilon_{\mathbf{k}}$, $\varepsilon_{\mathbf{k}}^{(2)} = -\varepsilon_{\mathbf{k}}^{(5)} = -\varepsilon_{\mathbf{k}}^+$, and $\varepsilon_{\mathbf{k}}^{(3)} = -\varepsilon_{\mathbf{k}}^{(4)} = -\varepsilon_{\mathbf{k}}^-$, with $\varepsilon_{\mathbf{k}} \geq \varepsilon_{\mathbf{k}}^+ \geq \varepsilon_{\mathbf{k}}^- \geq 0$. In each unit cell, six Majorana fermions are defined, but the number of the corresponding fermions are three. Thus, the lowest three bands should be filled for the ground state: $|g\rangle = \prod_{\mathbf{k}} \prod_{j=1}^3 \sqrt{2} A_{\mathbf{k}}^{(j)\dagger} |0\rangle$, with $\sqrt{2}$ the normalization factor which results from the fact that the fermion $A_{\mathbf{k}}^{(j)}$ is constructed from Majorana fermions in \mathbf{k} space, each of whom can only take 1/2 as its occupation number. The ground-state energy per site is given by $E_g = \frac{1}{6N} \sum_{\mathbf{k}} \left[\varepsilon_{\mathbf{k}}^{(1)} + \varepsilon_{\mathbf{k}}^{(2)} + \varepsilon_{\mathbf{k}}^{(3)} \right]$, where N is the number of unit cells. The energy-band gap, i.e., the minimal energy to excite a fermion from the ground state is $\Delta = \mathcal{M}[\varepsilon_{\mathbf{k}}^{(4)} - \varepsilon_{\mathbf{k}}^{(3)}]$, where $\mathcal{M}[\dots]$ denotes the minimal value of a function with variable \mathbf{k} .

Below we show the ground-state phase diagrams in two different parameter regimes. The first diagram contains critical curves separating two phases of either the same or different Chern numbers. This unveils that QPTs can also occur in the same topological class. The second diagram contains critical points where four different phases with Chern numbers 0, 0, 1 and -1 terminate.

III. CASE A: $J_x = J_y$, $J'_x = J'_y$, AND $J_z J'_x = J'_z J_x$

We first choose parameters $\Lambda_1 \equiv J'_x/J_x$, and $\Lambda_2 \equiv J_z/J_x$ to study the ground-state property of the system. In particular, the parameters with $\Lambda_2 = 1$ and $\Lambda_1 > 0$ correspond to the case studied in Ref. 5 where a topological QPT between an Abelian phase and a non-Abelian phase was found at point $\Lambda_1 = \sqrt{3}$. There is also a perturbative study¹³ of this model with parameters either $\Lambda_1 \ll 1$ or $\Lambda_1 \gg 1$ when $\Lambda_2 = 1$.

In order to find the ground-state phase diagram of the Kitaev spin model, we should first distinguish the gapless-phase regions from the gapped-phase regions in the phase diagram. Then, we calculate the Chern number^{14,15} as a topological index to characterize each gapped-phase region. We note that the six energy bands satisfy the relation $\varepsilon_{\mathbf{k}}^{(j)} = -\varepsilon_{\mathbf{k}}^{(7-j)}$, where $j = 1, 2, 3$, which implies that the closing of the energy-band gap corresponds to either $\mathcal{M}[-\varepsilon_{\mathbf{k}}^{(3)}] = 0$ or $\mathcal{M}[\varepsilon_{\mathbf{k}}^{(4)}] = 0$. Combining this condition with the relation $\varepsilon_{\mathbf{k}}^{(j)} = -\varepsilon_{\mathbf{k}}^{(7-j)}$, we can derive that if one has $\mathcal{M}[-\prod_{j=1}^6 \varepsilon_{\mathbf{k}}^{(j)}] = 0$, the

energy-band gap is zero, i.e., $\Delta = 0$. This gives rise to

$$\Lambda_1 = 0; \Lambda_2 = 0; \Lambda_1^2 = \Lambda_2^2 \pm \frac{2}{|\Lambda_2|}, \quad (4)$$

where $+$ ($-$) applies when $|\Lambda_1| > |\Lambda_2|$ ($|\Lambda_1| < |\Lambda_2|$). In Fig. 2(a), each gapless phase determined by Eq. (4) is schematically shown by a solid curve or line. One can see that the $\Lambda_1\Lambda_2$ plane is divided into 12 distinct regions by these solid curves or lines. Each of these 12 regions is a gapped topological phase and can be characterized by a Chern number.

We can define the Chern number by using the Berry's phase for a gapped ground state.^{14,15} Among the six bands of Hamiltonian (3), the lower three bands with states $|j, \mathbf{k}\rangle = \sqrt{2}A_{\mathbf{k}}^{(j)\dagger}|0\rangle$, where $j = 1, 2, 3$, are occupied. The Berry's phase gauge field in momentum space is

$$f_\alpha(\mathbf{k}) = -i \sum_{j=1}^3 \left\langle j, \mathbf{k} \left| \frac{\partial}{\partial k_\alpha} \right| j, \mathbf{k} \right\rangle, \quad (5)$$

where $\alpha = x, y$. This gives

$$\nu = \frac{1}{\pi} \text{Im} \sum_{s=1}^6 \sum_{i=1}^3 \int_{\text{BZ}} d^2k \left[\frac{\partial w_s^*(\varepsilon_{\mathbf{k}}^{(i)})}{\partial k_x} \frac{\partial w_s(\varepsilon_{\mathbf{k}}^{(i)})}{\partial k_y} \right], \quad (6)$$

where Im denotes the imaginary part of a complex variable. Numerical results show that each yellow (red) region in Fig. 2(a) corresponds to a gapped non-Abelian phases with Chern number $\nu = 1$ (-1). The other 8 white regions correspond to the Abelian phases with $\nu = 0$. A remarkable feature is that a critical curve or line (i.e. gapless phase) can separate two gapped phases with Chern numbers $\nu =$ (i) 0 and ± 1 , (ii) 0 and 0, or (iii) 1(-1) and ± 1 . This reveals that a QPT can occur between two gapped phases belonging to the same topological class.

Below we explicitly display the QPTs (see Fig. 3). As in Ref. 16, here we classify the QPTs as two types: The *first-order* QPT where the first derivative of the ground-state energy E_g with respect to the driving parameter is discontinuous at the transition point, and the *continuous* QPT where a higher-order derivative of E_g is discontinuous and the derivative(s) with order(s) lower is (are) continuous. Figure 3(a) [3(b)] shows that there is a first-order QPT between two phases of the *same* Chern number $\nu = 1$ (0) at $(\Lambda_1, \Lambda_2) = (0, 1)$ [(0, 2)], when one parameter varies along the horizontal dashed (dotted) line in Fig. 2(a). Using the perturbation method in 3, the effective Hamiltonian at $\Lambda_1 \sim 0$ can be obtained, up to third order, as (see Appendix B)

$$H_{\text{eff}} = H_0^{(3)} + \frac{6\Lambda_1^3}{\Lambda_2} \sum_n \left[P_1(n) \sigma_i^x \sigma_j^y \sigma_k^z + P_2(n) \sigma_{i'}^x \sigma_{j'}^y \sigma_{k'}^z \right], \quad (7)$$

where n denotes the n th unit cell, $H_0^{(3)}$ is a term containing none of P_0 , P_1 or P_2 , and the subscripts i, j , and k

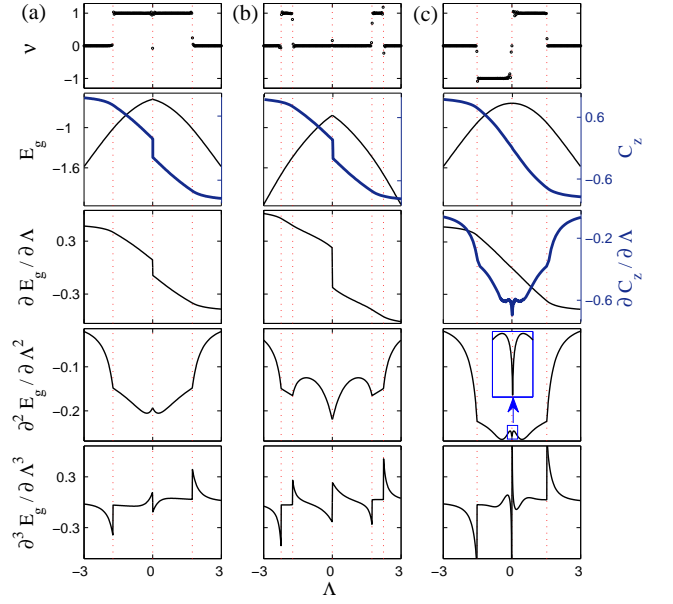


FIG. 3: (Color online) Chern number ν , the ground-state energy E_g and its derivatives, and the spin-spin correlation function C_z and its derivative with respect to the driving parameter. (a) $\Lambda = \Lambda_1$ and $\Lambda_2 = 1$; (b) $\Lambda = \Lambda_1$ and $\Lambda_2 = 2$; (c) $\Lambda = \Lambda_2$ and $\Lambda_1 = 1$. The parameters in (a), (b) and (c) correspond to the horizontal dashed, horizontal dotted and vertical dashed lines in Fig. 2(a).

(i' , j' , and k') denote the sites linked to plaquette P_1 (P_2) with x -, y - and z -link, respectively. For the QPT between two phases of the same Chern number, the parameter Λ_1 changes its sign at the transition point $\Lambda_1 = 0$. This gives rise to different H_{eff} 's at the two sides of the transition point $\Lambda_1 = 0$. Also, the difference between the two phases of the same Chern number but with positive and negative Λ_1 's can be seen from their wavefunctions (see Appendix A).

Using Feynmann theorem,⁹ it can be derived that

$$\frac{\partial E_g}{\partial \Lambda_1} = \frac{1}{6} (C_x + C_y + \Lambda_2 C_z), \quad (8)$$

where the spin-spin correlation functions are defined by $C_\alpha = \langle g | \sigma_i^\alpha \sigma_j^\alpha | g \rangle_{\alpha' \text{-link}}$, with $\alpha = x, y$ and z for $\alpha' = x', y'$ and z' . It is clear that the discontinuity of $\partial E_g / \partial \Lambda_1$ at a QPT point results from the discontinuity of C_α there. Here we find that, at the QPT point, the *nonlocal* spin-spin correlation function on the x' -, y' -, or z' -link changes its sign, displaying discontinuity there. As shown in Fig. 3(a) [Fig. 3(b)], C_z indeed has a jump at the QPT point $(\Lambda_1, \Lambda_2) = (0, 1)$ [(0, 2)] when Λ_1 changes from positive to negative. It should be noted that only part of the spin-spin couplings in the Hamiltonian (1) change their sign at these transition points, while the other spin-spin couplings are kept unchanged.

In addition to the first-order QPTs, continuous QPTs can also occur in the Kitaev spin model on a triangle-honeycomb lattice. As shown in Fig. 3 (a), $\partial E_g / \partial \Lambda_1$

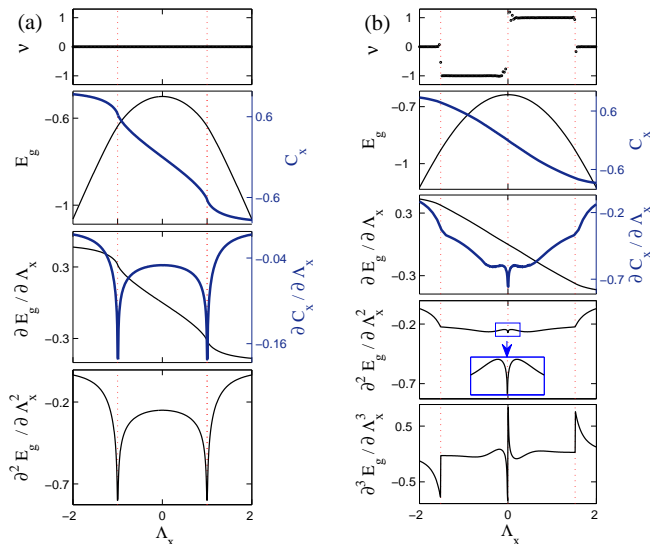


FIG. 4: (Color online) Chern number ν , the ground-state energy E_g , the spin-spin correlation function C_x , and the derivatives of both E_g and C_x with respect to the driving parameter Λ_x . The parameters in (a) and (b) correspond to the dashed and dotted lines in Fig. 2(b).

and $\partial^2 E_g / \partial \Lambda_1^2$ are continuous while $\partial^3 E_g / \partial \Lambda_1^3$ becomes discontinuous at $(\Lambda_1, \Lambda_2) = (\pm\sqrt{3}, 1)$. This corresponds to a topological QPT between Abelian and non-Abelian phases. Figure 3(b) shows that such a continuous QPT can also happen at $(\Lambda_1, \Lambda_2) = (\pm\sqrt{3}, 2)$ or $(\pm\sqrt{5}, 2)$. Similar to the first-order QPTs, the continuous QPTs result from the discontinuity of the second derivative of spin-spin correlation functions at the critical point.

Figure 3(c) displays three continuous QPTs. Interestingly, the QPT at $(\Lambda_1, \Lambda_2) = (1, 0)$, where $\partial^2 E_g / \partial \Lambda_2^2$ diverges, occurs between two non-Abelian phases with Chern numbers 1 and -1 , respectively. This is in sharp contrast to the other two QPTs occurring at $\Lambda_1 = 1$ and $\Lambda_2 \approx \pm 1.5$, where $\partial^3 E_g / \partial \Lambda_2^3$ is discontinuous and each transition is between Abelian and non-Abelian phases, instead of two non-Abelian phases. Also, it can be derived that

$$\frac{\partial E_g}{\partial \Lambda_2} = \frac{1}{6}(B_z + \Lambda_1 C_z), \quad (9)$$

where $B_z = \langle g | \sigma_i^z \sigma_j^z | g \rangle_{z\text{-link}}$. This unveils that the non-analyticity of E_g results from the nonanalyticity of either B_z or C_z . Indeed, Fig. 3(c) shows that $\partial C_z / \partial \Lambda_2$ is divergent at $(\Lambda_1, \Lambda_2) = (1, 0)$. Such a QPT between two phases of Chern numbers $\nu = \pm 1$ can also occur when changing the sign of the magnetic-field-related parameter κ in the Kitaev spin model on a honeycomb lattice.³

IV. CASE B: $J_\alpha = J'_\alpha$, WHERE $\alpha = x, y$, AND z

Here we use parameters $\Lambda_x \equiv J_x / J_z$, and $\Lambda_y \equiv J_y / J_z$ to characterize the phase diagram. The gapless-phase

curves determined by $\mathcal{M}[-\prod_{j=1}^6 \varepsilon_{\mathbf{k}}^{(j)}] = 0$ are

$$\begin{aligned} |\Lambda_y| &= \sqrt[3]{T_2^+ + T_1^+} + \sqrt[3]{T_1^+ - T_2^+}, \quad |\Lambda_y| > |\Lambda_x|; \\ |\Lambda_y| &= \sqrt[3]{T_2^- - T_1^-} - \sqrt[3]{T_2^- + T_1^-}, \quad |\Lambda_x| > |\Lambda_y|; \quad (10) \\ |\Lambda_y| &= \sqrt[3]{T_2^- + T_1^-} - \sqrt[3]{T_2^- - T_1^-}, \quad 1 \geq |\Lambda_x|, |\Lambda_y|. \end{aligned}$$

Here $T_1^\pm = (1 \pm |\Lambda_x|^3)/2$, and $T_2^\pm = \sqrt{(T_1^\pm)^2 \mp (|\Lambda_x|/3)^3}$. The gapless phase determined by each condition in Eq. (11) is shown by a solid curve in Fig 2(b). These gapless-phase curves divide the $\Lambda_x \Lambda_y$ plane into 9 regions: Two phases of Chern number $\nu = 1$ (-1), denoted by yellow (red) regions, and five gapped phases of Chern number $\nu = 0$, denoted by white regions. In this phase diagram, four gapped phases with $\nu = 0, 0, 1$ and -1 all terminate at a gapless-phase point $(\Lambda_x, \Lambda_y) = (0, \pm 1)$ or $(\pm 1, 0)$. Such a point is analogous to the eutectic point in crystallography. Also, a similar critical point exists in the phase diagram of the Haldane model.¹⁷

Below we focus on the QPTs at the points where different gapped phases terminate. When Λ_x varies along the dashed line in Fig. 2(b), a continuous QPT occurs at point $(\Lambda_x, \Lambda_y) = (\pm 1, 0)$, where $\partial^2 E_g / \partial \Lambda_x^2$ diverges [see Fig. 4(a)]. Similar to the QPT between two non-Abelian phases belonging to the same topological class, this QPT involves two Abelian phases with the same Chern number $\nu = 0$. When Λ_x varies along the dotted line in Fig. 2(b), in addition to the continuous QPTs between Abelian and non-Abelian phases (which occur at $\Lambda_x \approx \pm 1.5$ and $\Lambda_y = 1$, where $\partial^3 E_g / \partial \Lambda_x^3$ are discontinuous), a continuous QPT between two non-Abelian phases happens at point $(\Lambda_x, \Lambda_y) = (0, 1)$, where $\partial^2 E_g / \partial \Lambda_x^2$ diverges. In contrast to the QPT between two non-Abelian phases belonging to the same topological class, this transition involves two non-Abelian phases with $\nu = \pm 1$. Analogous to the first-order QPTs occurring in the same topological class (Fig. 3), the continuous QPTs here are also due to the singularity of the nonlocal correlation functions at the critical points (see, e.g., the thick solid curves in Fig. 4).

V. CONCLUSION

We have studied QPTs in the Kitaev spin model on a triangle-honeycomb lattice and revealed the exotic ground-state phase diagram of this model. In addition to the ordinary topological QPTs between Abelian and non-Abelian phases, we find new QPTs that occur between two phases belonging to the same topological class. Moreover, we show that such QPTs are due to the singular behaviors of the nonlocal spin-spin correlation functions at the critical points.

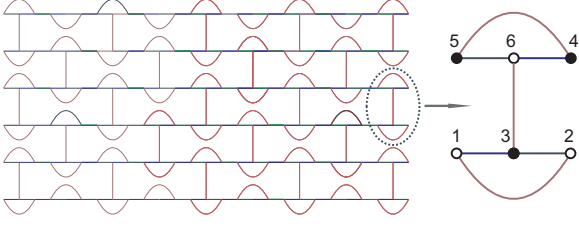


FIG. 5: (Color online) The triangle-honeycomb lattice in Fig. 1(a) is deformed to a topologically equivalent lattice, so as to label each site by row and column indices. In each unit cell, the three sites denoted by 3, 4, and 5 have row and column indices m and n with $m + n$ equal to an even integer, and the other three sites denoted by 1, 2, and 6 have row and column indices with $m + n$ equal to an odd integer.

Acknowledgments

This work was supported by the National Basic Research Program of China under Grant No. 2009CB929300, and the National Natural Science Foundation of China under Grant No. 10625416.

Appendix A

1. Derivation of the ground state in the uniform-flux sector

The Kitaev spin model on a triangle-honeycomb lattice is schematically shown in Fig. 5 and the model Hamiltonian is given by

$$\begin{aligned}
 H = & J_x \sum_{x\text{-link}} \sigma_i^x \sigma_j^x + J_y \sum_{y\text{-link}} \sigma_i^y \sigma_j^y + J_z \sum_{z\text{-link}} \sigma_i^z \sigma_j^z \\
 & + J'_x \sum_{x'\text{-link}} \sigma_i^x \sigma_j^x + J'_y \sum_{y'\text{-link}} \sigma_i^y \sigma_j^y + J'_z \sum_{z'\text{-link}} \sigma_i^z \sigma_j^z.
 \end{aligned} \quad (\text{A1})$$

To use the Jordan-Wigner transformation, we need to label the sites by row and column indices. We deform the honeycomb lattice [see Fig 1(a)] into the topologically equivalent one in Fig. 5. Now each site can be labeled by (m, n) , where m ($= 1, 2, \dots, M$) and n ($= 1, 2, \dots, N$) are the row and column indices, respectively.

By performing the Jordan-Wigner transformation¹⁸

$$\sigma_{m,n}^+ = 2a_{m,n}^\dagger \prod_{n'=1}^n \prod_{m'<m} \sigma_{m',n'}^z \prod_{n''<n} \sigma_{m,n''}^z \quad (\text{A2})$$

on each spin, and using the Majorana fermions

$$c_{m,n}^{(s)} \equiv i(a_{m,n}^\dagger - a_{m,n}), \quad d_{m,n}^{(s)} \equiv a_{m,n}^\dagger + a_{m,n} \quad (\text{A3})$$

for sites $s = 3, 4, 5$, and

$$c_{m,n}^{(s)} \equiv a_{m,n}^\dagger + a_{m,n}, \quad d_{m,n}^{(s)} \equiv i(a_{m,n}^\dagger - a_{m,n}) \quad (\text{A4})$$

for sites $s = 1, 2, 6$ in each unit cell [see Fig. 5], the Hamiltonian (A1) is converted to

$$\begin{aligned}
 H = & iJ_x \left[\sum_{x\text{-link}(\Delta)} c_{m,n}^{(3)} c_{m,n+1}^{(2)} + \sum_{x\text{-link}(\nabla)} c_{m,n}^{(5)} c_{m,n+1}^{(6)} \right] \\
 & - iJ_y \left[\sum_{y\text{-link}(\Delta)} c_{m,n}^{(1)} c_{m,n+1}^{(3)} + \sum_{y\text{-link}(\nabla)} c_{m,n}^{(6)} c_{m,n+1}^{(4)} \right] \\
 & + iJ'_x \sum_{x'\text{-link}, n \neq N} c_{m,n}^{(4)} c_{m,n+1}^{(1)} \\
 & - iJ'_y \sum_{y'\text{-link}, n \neq N} c_{m,n}^{(2)} c_{m,n+1}^{(5)} \\
 & + iJ'_x \sum_{m=1}^{M/2} \Phi_{x,2m} c_{2m,N}^{(4)} c_{2m,1}^{(1)} \\
 & - iJ'_y \sum_{m=1}^{M/2} \Phi_{x,2m-1} c_{2m-1,N}^{(2)} c_{2m-1,1}^{(5)} \\
 & + iJ_z \sum_{z\text{-link}(\Delta)} i d_{m,n}^{(1)} d_{m,n+2}^{(2)} c_{m,n}^{(1)} c_{m,n+2}^{(2)} \\
 & + iJ_z \sum_{z\text{-link}(\nabla)} i d_{m,n+2}^{(4)} d_{m,n}^{(5)} c_{m,n+2}^{(4)} c_{m,n}^{(5)} \\
 & + iJ'_z \sum_{z'\text{-link}} i d_{m,n}^{(3)} d_{m+1,n}^{(6)} c_{m,n}^{(3)} c_{m+1,n}^{(6)}, \quad (\text{A5})
 \end{aligned}$$

where $\Phi_{x,m} = \prod_{n=1}^N \sigma_{m,n}^z$, $m = 1, 2, \dots$, or M , is the global flux operator calculated along a given contour encircling the system in the horizontal direction, $\alpha\text{-link}(\Delta)$ denotes the α -link in an up-pointing triangle, and $\alpha\text{-link}(\nabla)$ the α -link in a down-pointing triangle.

The global flux operator calculated along a given contour encircling the system in the vertical direction, which does not appear in the Hamiltonian (A5), is given by

$$\begin{aligned}
 \Phi_{y,n} = & \prod_{m=0}^{M/2-1} \sigma_{1+2m,n}^y \sigma_{2+2m,n}^x \sigma_{2+2m,n+1}^z \sigma_{2+2m,n+2}^z \\
 & \otimes \sigma_{2+2m,n+3}^x \sigma_{3+2m,n+3}^y \sigma_{3+2m,n+2}^z \sigma_{3+2m,n+1}^z \\
 = & (-1)^{\frac{M}{2}} \prod_{m=0}^{M/2-1} d_{1+2m,n}^{(3)} d_{2+2m,n}^{(6)} d_{2+2m,n+3}^{(3)} \\
 & \otimes d_{3+2m,n+3}^{(6)}, \quad (\text{A6})
 \end{aligned}$$

where $n = 1 + 6r$ with $r = 0, 1, \dots$, or $N/6 - 1$. These two global flux operators $\Phi_{x,m}$ and $\Phi_{y,n}$ commute with Hamiltonian (A1). This leads to a topological degeneracy for the ground state because $\Phi_{x,m}$ and $\Phi_{y,n}$ can have eigenvalues either 1 or -1 . For the Abelian phase, this degeneracy is 4-fold because $(\Phi_{x,m}, \Phi_{y,n})$ can be $(1, 1)$, $(1, -1)$, $(-1, 1)$, and $(-1, -1)$, while the degeneracy is 3-fold for the non-Abelian phase since $(\Phi_{x,m}, \Phi_{y,n}) = (-1, -1)$ is not allowed.⁵ In addition to the global flux operators, the three types of local plaquette operators P_0 , P_1 , and P_2 also commute with Hamiltonian (A1).

Using the Jordan-Wigner transform, they can be written as

$$\begin{aligned}
P_0(m, n) &= d_{m,n}^{(3)} d_{m+1,n}^{(6)} d_{m,n+6}^{(3)} d_{m+1,n+6}^{(6)} \\
&\quad \otimes P_1(m, n+2) P_2(m+1, n+2), \\
P_1(m', n') &= i d_{m',n'+2}^{(4)} d_{m',n'}^{(5)}, \\
P_2(m'', n'') &= i d_{m'',n''}^{(1)} d_{m'',n''+2}^{(2)}, \tag{A7}
\end{aligned}$$

where (m, n) , (m', n') , and (m'', n'') correspond, respectively, to the sites denoted by 3, 5, and 1 in each unit cell. As shown in Ref. 5, the ground state lies in the sector of the Hilbert space where either (i) $P_0(m, n) = 1$ and $P_1(m', n') = P_2(m'', n'') = 1$ or (ii) $P_0(m, n) = 1$ and $P_1(m', n') = P_2(m'', n'') = -1$. In each of these two sectors, the time reversal symmetry of Hamiltonian (A1) is broken. The former is called as the uniform-flux sector. This means that the ground state has another 2-fold degeneracy due to this broken time reversal symmetry, in addition to the topological degeneracy discussed above. Thus, we have 8-fold (6-fold) degeneracy for the ground state in the Abelian (non-Abelian) phase, corresponding to 8 (6) flux configurations for $\Phi_{x,m}, \Phi_{y,n}, P_0, P_1$, and P_2 .

Here we focus on the ground state in the uniform-flux sector with $(\Phi_{x,m}, \Phi_{y,n}) = (1, 1)$, which allow both Abelian and non-Abelian phases.⁵ Note that only one ground state exists in this sector. Now, Hamiltonian (A5) is reduced to

$$\begin{aligned}
H_u &= iJ_x \left[\sum_{x\text{-link}(\Delta)} c_{m,n}^{(3)} c_{m,n+1}^{(2)} + \sum_{x\text{-link}(\nabla)} c_{m,n}^{(5)} c_{m,n+1}^{(6)} \right] \\
&\quad - iJ_y \left[\sum_{y\text{-link}(\Delta)} c_{m,n}^{(1)} c_{m,n+1}^{(3)} + \sum_{y\text{-link}(\nabla)} c_{m,n}^{(6)} c_{m,n+1}^{(4)} \right] \\
&\quad + iJ_z \left[\sum_{z\text{-link}(\Delta)} c_{m,n}^{(1)} c_{m,n+2}^{(2)} + \sum_{z\text{-link}(\nabla)} c_{m,n+2}^{(4)} c_{m,n}^{(5)} \right]
\end{aligned}$$

$$H_{\mathbf{k}} = \begin{pmatrix} 0 & iJ_z & -iJ_y & -iJ'_x e^{i\mathbf{k}\cdot\mathbf{e}_2} & 0 & 0 \\ -iJ_z & 0 & -iJ_x & 0 & -iJ'_y e^{-i\mathbf{k}\cdot\mathbf{e}_1} & 0 \\ iJ_y & iJ_x & 0 & 0 & 0 & iJ'_z \\ iJ'_x e^{-i\mathbf{k}\cdot\mathbf{e}_2} & 0 & 0 & 0 & iJ_z & iJ_y \\ 0 & iJ'_y e^{i\mathbf{k}\cdot\mathbf{e}_1} & 0 & -iJ_z & 0 & iJ_x \\ 0 & 0 & -iJ'_z & -iJ_y & -iJ_x & 0 \end{pmatrix}. \tag{A13}$$

From the eigenvalue equation $H_{\mathbf{k}}\Psi = \varepsilon_{\mathbf{k}}\Psi$, one has

$$\varepsilon_{\mathbf{k}}^6 - a\varepsilon_{\mathbf{k}}^4 + b\varepsilon_{\mathbf{k}}^2 - c = 0, \tag{A14}$$

where

$$\begin{aligned}
a &= 2(J_x^2 + J_y^2 + J_z^2) + J'_x{}^2 + J'_y{}^2 + J'_z{}^2, \\
b &= 2(J_x^2 J_y^2 + J_y^2 J_z^2 + J_z^2 J_x^2 + J_x^2 J'_x{}^2 + J_y^2 J'_y{}^2 + J_z^2 J'_z{}^2)
\end{aligned}$$

$$\begin{aligned}
&+ iJ'_x \sum_{x'\text{-link}} c_{m,n}^{(4)} c_{m,n+1}^{(1)} - iJ'_y \sum_{y'\text{-link}} c_{m,n}^{(2)} c_{m,n+1}^{(5)} \\
&+ iJ'_z \sum_{z'\text{-link}} c_{m,n}^{(3)} c_{m+1,n}^{(6)}. \tag{A8}
\end{aligned}$$

By using the Fourier transform

$$\begin{aligned}
c_{\mathbf{r}}^{(s)} &= \sqrt{\frac{12}{NM}} \sum_{\mathbf{k} \in \text{BZ}} e^{i\mathbf{k}\cdot\mathbf{r}} c_{\mathbf{k}}^{(s)}, \\
c_{\mathbf{k}}^{(s)} &= \sqrt{\frac{3}{NM}} \sum_{\mathbf{r}} e^{-i\mathbf{k}\cdot\mathbf{r}} c_{\mathbf{r}}^{(s)}, \tag{A9}
\end{aligned}$$

which satisfies

$$\left\{ c_{\mathbf{r}}^{(s)}, c_{\mathbf{r}'}^{(s')} \right\} = 2\delta_{\mathbf{r},\mathbf{r}'} \delta_{s,s'}, \quad \left\{ c_{\mathbf{k}}^{(s)}, c_{\mathbf{k}'}^{(s')} \right\} = \delta_{\mathbf{k},-\mathbf{k}'} \delta_{s,s'}, \tag{A10}$$

where BZ denotes the first Brillouin zone, $s = 1, 2, \dots, 6$ denote the six sites in each unit cell, and \mathbf{r} is the position of a unit cell, Eq. (A8) becomes

$$\begin{aligned}
H_u &= 2i \sum_{\mathbf{k} \in \text{BZ}} \left\{ J'_x e^{-i\mathbf{k}\cdot\mathbf{e}_2} c_{\mathbf{k}}^{(4)} c_{-\mathbf{k}}^{(1)} + J_x \left[c_{\mathbf{k}}^{(5)} c_{-\mathbf{k}}^{(6)} + c_{\mathbf{k}}^{(3)} c_{-\mathbf{k}}^{(2)} \right] \right. \\
&\quad \left. - J'_y e^{-i\mathbf{k}\cdot\mathbf{e}_1} c_{\mathbf{k}}^{(2)} c_{-\mathbf{k}}^{(5)} - J_y \left[c_{\mathbf{k}}^{(1)} c_{-\mathbf{k}}^{(3)} + c_{\mathbf{k}}^{(6)} c_{-\mathbf{k}}^{(4)} \right] \right. \\
&\quad \left. + J'_z c_{\mathbf{k}}^{(3)} c_{-\mathbf{k}}^{(6)} + J_z \left[c_{\mathbf{k}}^{(1)} c_{-\mathbf{k}}^{(2)} + c_{\mathbf{k}}^{(4)} c_{-\mathbf{k}}^{(5)} \right] \right\}, \tag{A11}
\end{aligned}$$

where $c_{-\mathbf{k}}^{(s)} = c_{\mathbf{k}}^{(s)\dagger}$, and the two basis vectors of the unit cell are $\mathbf{e}_1 = \mathbf{e}_x/2 - \sqrt{3}\mathbf{e}_y/2$, and $\mathbf{e}_2 = \mathbf{e}_x/2 + \sqrt{3}\mathbf{e}_y/2$. To obtain the quasi-particle spectrum, we write Eq. (A11) as

$$H_u = \sum_{\mathbf{k} \in \text{BZ}} \Phi_{\mathbf{k}}^\dagger H_{\mathbf{k}} \Phi_{\mathbf{k}}, \tag{A12}$$

where $\Phi_{\mathbf{k}}^\dagger = (c_{\mathbf{k}}^{(1)}, c_{\mathbf{k}}^{(2)}, c_{\mathbf{k}}^{(3)}, c_{\mathbf{k}}^{(4)}, c_{\mathbf{k}}^{(5)}, c_{\mathbf{k}}^{(6)})$, and

$$\begin{aligned}
&+ J_x^2 J_y^2 + J_y^2 J_z^2 + J_z^2 J_x^2 + J_x^4 + J_y^4 + J_z^4 \\
&- 2J'_x J'_y J_z^2 \cos k_x - 2J'_z J'_x J_y^2 \cos k_2 \\
&- 2J'_y J'_z J_x^2 \cos k_1, \\
c &= J_x^4 J_x^2 + J_y^4 J_y^2 + J_z^4 J_z^2 + J_x^2 J'_x{}^2 J_y^2 \\
&- 2J'_x J'_y (J_z^2 J_z^2 - J_x^2 J_y^2) \cos k_x
\end{aligned}$$

$$\begin{aligned}
& -2J'_y J'_z (J_x^2 J_x'^2 - J_y^2 J_z^2) \cos k_1 \\
& -2J'_z J'_x (J_y^2 J_y'^2 - J_z^2 J_x^2) \cos k_2,
\end{aligned} \tag{A15}$$

with

$$k_1 = \frac{k_x - \sqrt{3}k_y}{2}, \quad k_2 = \frac{k_x + \sqrt{3}k_y}{2}. \tag{A16}$$

The solution of Eq. (A14) reads

$$\begin{aligned}
\varepsilon_{\mathbf{k}}^{(1)} &= -\varepsilon_{\mathbf{k}}^{(6)} = -\sqrt{\frac{a}{3} + 2p \cos \varphi}, \\
\varepsilon_{\mathbf{k}}^{(2)} &= -\varepsilon_{\mathbf{k}}^{(5)} = -\sqrt{\frac{a}{3} - p (\cos \varphi - \sqrt{3} \sin \varphi)}, \\
\varepsilon_{\mathbf{k}}^{(3)} &= -\varepsilon_{\mathbf{k}}^{(4)} = -\sqrt{\frac{a}{3} - p (\cos \varphi + \sqrt{3} \sin \varphi)},
\end{aligned} \tag{A17}$$

where

$$\begin{aligned}
\varphi &= \frac{1}{3} \arccos \left(\frac{q}{2p^3} \right), \quad 0 \leq \varphi \leq \frac{\pi}{3}, \\
p &= \frac{1}{3} \sqrt{a^2 - 3b}, \quad q = \frac{2a^3}{27} - \frac{ab}{3} + c.
\end{aligned} \tag{A18}$$

With the six energy bands in Eq. (A17), the Hamiltonian (A13) can be written as

$$H_u = \sum_{j=1, \mathbf{k} \in \text{BZ}}^{j=3} \varepsilon_{\mathbf{k}}^{(j)} \left[2A_{\mathbf{k}}^{(j)\dagger} A_{\mathbf{k}}^{(j)} - 1 \right], \tag{A19}$$

where $A_{\mathbf{k}}^{(j)\dagger} = \sum_{s=1}^6 c_{\mathbf{k}}^{(s)} w_s(\varepsilon_{\mathbf{k}}^{(j)})$ is a fermionic operator, with $c_{\mathbf{k}}^{(s)}$ the Fourier transform of the Majorana fermionic operator at site s ($s = 1, 2, \dots, 6$) of the unit cell, and

$$w_s(\varepsilon_{\mathbf{k}}^{(j)}) = \frac{w'_s(\varepsilon_{\mathbf{k}}^{(j)})}{\sqrt{\sum_{i=1}^6 |w'_i(\varepsilon_{\mathbf{k}}^{(j)})|^2}}. \tag{A20}$$

In Eq. (A20),

$$\begin{aligned}
w'_1 &= \frac{iJ'_x}{W} \left[(\varepsilon_{\mathbf{k}}^{(j)})^2 - J_x^2 \right] e^{ik_2} w'_4 + \frac{iJ'_y}{W} \left(iJ_z \varepsilon_{\mathbf{k}}^{(j)} \right. \\
& \quad \left. + J_x J_y \right) e^{-ik_1} w'_5 + \frac{iJ'_z}{W} \left(iJ_y \varepsilon_{\mathbf{k}}^{(j)} - J_x J_z \right) w'_6, \\
w'_2 &= \frac{iJ'_x}{W} \left(J_x J_y - iJ_z \varepsilon_{\mathbf{k}}^{(j)} \right) e^{ik_2} w'_4 + \frac{iJ'_y}{W} \left[(\varepsilon_{\mathbf{k}}^{(j)})^2 \right. \\
& \quad \left. - J_y^2 \right] e^{-ik_1} w'_5 + \frac{iJ'_z}{W} \left(J_y J_z + iJ_x \varepsilon_{\mathbf{k}}^{(j)} \right) w'_6, \\
w'_3 &= \frac{iJ'_x}{W} \left(J_x J_z + iJ_y \varepsilon_{\mathbf{k}}^{(j)} \right) e^{ik_2} w'_4 + \frac{iJ'_y}{W} \left(iJ_x \varepsilon_{\mathbf{k}}^{(j)} \right. \\
& \quad \left. - J_y J_z \right) e^{-ik_1} w'_5 + \frac{iJ'_z}{W} \left[J_z^2 - (\varepsilon_{\mathbf{k}}^{(j)})^2 \right] w'_6, \\
w'_4 &= \frac{iJ_z W - J'_x J'_y \left(iJ_z \varepsilon_{\mathbf{k}}^{(j)} + J_x J_y \right) e^{-ik_x}}{\varepsilon_{\mathbf{k}}^{(j)} W + \left[(\varepsilon_{\mathbf{k}}^{(j)})^2 - J_x^2 \right] J_x'^2} w'_5
\end{aligned}$$

$$\begin{aligned}
& \frac{iJ_y W - J'_z J'_x \left(iJ_y \varepsilon_{\mathbf{k}}^{(j)} - J_x J_z \right) e^{-ik_2}}{\varepsilon_{\mathbf{k}}^{(j)} W + \left[(\varepsilon_{\mathbf{k}}^{(j)})^2 - J_x^2 \right] J_x'^2} w'_6, \\
w'_5 &= iJ_x J_x'^2 J'_y J'_z e^{ik_1} - J'_y J'_z \left(J_y J_z + iJ_x \varepsilon_{\mathbf{k}}^{(j)} \right) \varepsilon_{\mathbf{k}}^{(j)} e^{ik_1} \\
& \quad + iJ_x \left\{ \varepsilon_{\mathbf{k}}^{(j)} W + \left[(\varepsilon_{\mathbf{k}}^{(j)})^2 - J_x^2 \right] J_x'^2 \right\} \\
& \quad + J_y J_z W + iJ_z J'_z J'_x \left(-J_x J_z + iJ_y \varepsilon_{\mathbf{k}}^{(j)} \right) e^{-ik_2} \\
& \quad - iJ_y J'_x J'_y \left(J_x J_y - iJ_z \varepsilon_{\mathbf{k}}^{(j)} \right) e^{ik_x}, \\
w'_6 &= \left[(J_x^2 + J_y^2) (\varepsilon_{\mathbf{k}}^{(j)})^2 - J_x'^2 J_y'^2 - J_x^2 J_x'^2 - J_y^2 J_y'^2 \right] \varepsilon_{\mathbf{k}}^{(j)} \\
& \quad + \left[(\varepsilon_{\mathbf{k}}^{(j)})^2 - J_z^2 \right] W - J_z J'_x J'_y \left(2J_x J_y \sin k_x \right. \\
& \quad \left. - 2J_z \varepsilon_{\mathbf{k}}^{(j)} \cos k_x \right),
\end{aligned} \tag{A21}$$

with

$$W = \left[J_x^2 + J_y^2 + J_z^2 - (\varepsilon_{\mathbf{k}}^{(j)})^2 \right] \varepsilon_{\mathbf{k}}^{(j)}. \tag{A22}$$

In order to find the ground-state wavefunction for Hamiltonian (A19), we should first define the vacuum $|0\rangle$ by

$$a_{m,n}|0\rangle = 0, \tag{A23}$$

where $a_{m,n}$ is the fermionic operator defined in Eq. (A2), and the index (m, n) runs over every site of the lattice. From Eqs. (A3) and (A4), we have

$$\langle 0 | c_{\mathbf{r}}^{(s)} c_{\mathbf{r}'}^{(s')} | 0 \rangle = \delta_{\mathbf{r}, \mathbf{r}'} \delta_{s, s'}. \tag{A24}$$

Through Fourier transform, it leads to

$$\langle 0 | c_{\mathbf{k}}^{(s)} c_{\mathbf{k}'}^{(s')} | 0 \rangle = \frac{1}{2} \delta_{\mathbf{k}', -\mathbf{k}} \delta_{s', s}. \tag{A25}$$

For state $|j, \mathbf{k}\rangle = \sqrt{2} A_{\mathbf{k}}^{(j)\dagger} |0\rangle$ in the occupied band, it is normalized as

$$\begin{aligned}
\langle j, \mathbf{k} | j, \mathbf{k} \rangle &= \langle 0 | \sqrt{2} A_{\mathbf{k}}^{(j)} \sqrt{2} A_{\mathbf{k}}^{(j)\dagger} | 0 \rangle \\
&= 2 \sum_{s, s'=1}^6 w_s^*(\varepsilon_{\mathbf{k}}^{(j)}) w_{s'}(\varepsilon_{\mathbf{k}}^{(j)}) \langle 0 | c_{-\mathbf{k}}^{(s)} c_{\mathbf{k}}^{(s')} | 0 \rangle \\
&= 2 \sum_{s, s'=1}^6 w_s^*(\varepsilon_{\mathbf{k}}^{(j)}) w_{s'}(\varepsilon_{\mathbf{k}}^{(j)}) \cdot \frac{1}{2} \delta_{s', s} \\
&= \sum_{s=1}^6 |w_s(\varepsilon_{\mathbf{k}}^{(j)})|^2 \\
&= 1,
\end{aligned} \tag{A26}$$

which clarifies that the normalization factor $\sqrt{2}$ is due to the fact that the occupation number can only take 1/2 for the Fourier transform of each Majorana fermion [see Eq. (A25)]. Hence we can write the ground-state wavefunction as

$$|g\rangle = \prod_{\mathbf{k} \in \text{BZ}} \prod_{j=1}^3 \sqrt{2} A_{\mathbf{k}}^{(j)\dagger} |0\rangle. \tag{A27}$$

The corresponding ground-state energy per site is

$$\begin{aligned} E_g &= \frac{1}{6MN} \sum_{\mathbf{k} \in \text{BZ}} \left(\varepsilon_{\mathbf{k}}^{(1)} + \varepsilon_{\mathbf{k}}^{(2)} + \varepsilon_{\mathbf{k}}^{(3)} \right) \\ &= \frac{\sqrt{3}}{48\pi^2} \int_{\text{BZ}} d^2k \left(\varepsilon_{\mathbf{k}}^{(1)} + \varepsilon_{\mathbf{k}}^{(2)} + \varepsilon_{\mathbf{k}}^{(3)} \right). \end{aligned} \quad (\text{A28})$$

2. Two different ground states in the same topological class

Below we show that the quantum phase transition (QPT) between two phases belonging to the same topological class is nontrivial. For example, in the case of $J_x = J_y$, $J'_x = J'_y$, and $J_z J'_x = J'_z J_x$, the QPT that occurs when $\Lambda_1 \equiv J'_x/J_x$ varies across the critical line $\Lambda_1 = 0$ does not change the topological class of the ground state, i.e., the QPT occurs between either two non-Abelian phases with Chern number $\nu = \pm 1$ or two Abelian phases with $\nu = 0$. By using the parameters $\Lambda_1 \equiv J'_x/J_x$ and $\Lambda_2 \equiv J_z/J_x$, Eq. (A21) can be reduced to

$$\begin{aligned} w'_1 &= \frac{i\Lambda_1}{W'} \left\{ \left[(\varepsilon_{\mathbf{k}}^{(j)})^2 - 1 \right] e^{ik_2} w'_4 + \left(i\Lambda_2 \varepsilon_{\mathbf{k}}^{(j)} + 1 \right) e^{-ik_1} w'_5 \right. \\ &\quad \left. + \Lambda_2 \left(i\varepsilon_{\mathbf{k}}^{(j)} - \Lambda_2 \right) w'_6 \right\}, \\ w'_2 &= \frac{i\Lambda_1}{W'} \left\{ \left(1 - i\Lambda_2 \varepsilon_{\mathbf{k}}^{(j)} \right) e^{ik_2} w'_4 + \left[(\varepsilon_{\mathbf{k}}^{(j)})^2 - 1 \right] e^{-ik_1} w'_5 \right. \\ &\quad \left. + \Lambda_2 \left(\Lambda_2 + i\varepsilon_{\mathbf{k}}^{(j)} \right) w'_6 \right\}, \\ w'_3 &= \frac{i\Lambda_1}{W'} \left\{ \left(\Lambda_2 + i\varepsilon_{\mathbf{k}}^{(j)} \right) e^{ik_2} w'_4 + \left(i\varepsilon_{\mathbf{k}}^{(j)} - \Lambda_2 \right) e^{-ik_1} w'_5 \right. \\ &\quad \left. + \Lambda_2 \left[\Lambda_2^2 - (\varepsilon_{\mathbf{k}}^{(j)})^2 \right] w'_6 \right\}, \\ w'_4 &= \frac{i\Lambda_2 W' - \Lambda_1^2 \left(i\Lambda_2 \varepsilon_{\mathbf{k}}^{(j)} + 1 \right) e^{-ik_x}}{W' \varepsilon_{\mathbf{k}}^{(j)} + \left[(\varepsilon_{\mathbf{k}}^{(j)})^2 - 1 \right] \Lambda_1^2} w'_5 \\ &\quad + \frac{iW' - \Lambda_2 \left(i\varepsilon_{\mathbf{k}}^{(j)} - \Lambda_2 \right) e^{-ik_2}}{W' \varepsilon_{\mathbf{k}}^{(j)} + \left[(\varepsilon_{\mathbf{k}}^{(j)})^2 - 1 \right] \Lambda_1^2} w'_6, \\ w'_5 &= J_x^5 \left\{ i\Lambda_1^4 \Lambda_2 e^{ik_1} - \Lambda_1^2 \Lambda_2 \left(\Lambda_2 + i\varepsilon_{\mathbf{k}}^{(j)} \right) \varepsilon_{\mathbf{k}}^{(j)} e^{ik_1} + \Lambda_2 W' \right. \\ &\quad \left. + i\Lambda_1^2 \Lambda_2^2 \left(i\varepsilon_{\mathbf{k}}^{(j)} - \Lambda_2 \right) e^{-ik_2} - i\Lambda_1^2 \left(1 - i\Lambda_2 \varepsilon_{\mathbf{k}}^{(j)} \right) e^{ik_x} \right. \\ &\quad \left. + i \left[W' \varepsilon_{\mathbf{k}}^{(j)} + \Lambda_1^2 (\varepsilon_{\mathbf{k}}^{(j)})^2 - \Lambda_1^2 \right] \right\}, \\ w'_6 &= J_x^5 \left\{ \Lambda_1^2 \left[2(\varepsilon_{\mathbf{k}}^{(j)})^2 - \Lambda_1^2 - 2\Lambda_2^2 \right] \varepsilon_{\mathbf{k}}^{(j)} + \left[(\varepsilon_{\mathbf{k}}^{(j)})^2 \right. \right. \\ &\quad \left. \left. - \Lambda_2^2 \right] W' - \Lambda_1^2 \Lambda_2 \left(2 \sin k_x - 2\Lambda_2 \varepsilon_{\mathbf{k}}^{(j)} \cos k_x \right) \right\} \end{aligned} \quad (\text{A29})$$

with

$$W' = \left[2 + \Lambda_2^2 - (\varepsilon_{\mathbf{k}}^{(j)})^2 \right] \varepsilon_{\mathbf{k}}^{(j)}, \quad (\text{A30})$$

where $\varepsilon_{\mathbf{k}}^{(j)}$ is in units of J_x . These w'_s satisfy

$$w'_s(-\Lambda_1, \Lambda_2) = -w'_s(\Lambda_1, \Lambda_2), \quad s = 1, 2, 3;$$

$$w'_s(-\Lambda_1, \Lambda_2) = w'_s(\Lambda_1, \Lambda_2), \quad s = 4, 5, 6. \quad (\text{A31})$$

From $A_{\mathbf{k}}^{(i)\dagger} = \sum_{s=1}^6 c_{\mathbf{k}}^{(s)} w_s(\varepsilon_{\mathbf{k}}^{(j)})$, where w_s are given in Eq. (A20), we can define an analytical function $F \left(c_{\mathbf{k}}^{(1)}, c_{\mathbf{k}}^{(2)}, c_{\mathbf{k}}^{(3)}, c_{\mathbf{k}}^{(4)}, c_{\mathbf{k}}^{(5)}, c_{\mathbf{k}}^{(6)} \right)$ by

$$\begin{aligned} |g(\Lambda_1, \Lambda_2)\rangle &= \prod_{\mathbf{k} \in \text{BZ}} \prod_{j=1}^3 \sqrt{2} A_{\mathbf{k}}^{(j)\dagger} |0\rangle \\ &\equiv \prod_{\mathbf{k} \in \text{BZ}} F \left(c_{\mathbf{k}}^{(1)}, c_{\mathbf{k}}^{(2)}, c_{\mathbf{k}}^{(3)}, c_{\mathbf{k}}^{(4)}, c_{\mathbf{k}}^{(5)}, c_{\mathbf{k}}^{(6)} \right) |0\rangle. \end{aligned} \quad (\text{A32})$$

From Eq. (A31), it follows that

$$\begin{aligned} |g(-\Lambda_1, \Lambda_2)\rangle &= \prod_{\mathbf{k} \in \text{BZ}} F \left(-c_{\mathbf{k}}^{(1)}, -c_{\mathbf{k}}^{(2)}, -c_{\mathbf{k}}^{(3)}, c_{\mathbf{k}}^{(4)}, c_{\mathbf{k}}^{(5)}, c_{\mathbf{k}}^{(6)} \right) |0\rangle \end{aligned} \quad (\text{A33})$$

Equations (A32) and (A33) show that the ground state $|g(\Lambda_1, \Lambda_2)\rangle$ is mapped to $|g(-\Lambda_1, \Lambda_2)\rangle$ when $c_{\mathbf{k}}^{(s)}$, $s = 1, 2$, and 3, are changed to $-c_{\mathbf{k}}^{(s)}$. Because $c_{\mathbf{k}}^{(s)}$, $s = 1, 2$, and 3, are the Fourier transform of the Majorana fermions $c_{\mathbf{r}}^{(s)}$ defined on sites 1, 2, and 3 in each unit cell (i.e., all the triangles related to plaquette operator $P^{(2)}$). The transformation $c_{\mathbf{k}}^{(s)} \rightarrow -c_{\mathbf{k}}^{(s)}$ corresponds to a π phase change to each of the Majorana fermions $c_{\mathbf{r}}^{(s)}$ at sites $s = 1, 2$, and 3. Note that the two ground states $|g(\Lambda_1, \Lambda_2)\rangle$ and $|g(-\Lambda_1, \Lambda_2)\rangle$ are different [see Eqs. (A32) and (A33)], although the energy spectrum of the Hamiltonian $H(\Lambda_1, \Lambda_2)$ is symmetric about the critical line $\Lambda_1 = 0$.

Appendix B: Effective Hamiltonian

In order to show that both the QPTs between two Abelian phases and those between two non-Abelian phases are nontrivial, we use the perturbation method in Ref. 3 to derive the effective Hamiltonian at $\Lambda_1 \sim 0$. In this case with $J_x = J_y$, $J'_x = J'_y$, and $J_z J'_x = J'_z J_x$, we characterize the phase diagram by the two parameters $\Lambda_1 \equiv J'_x/J_x$, and $\Lambda_2 \equiv J_z/J_x$. We assume $J_x > 0$ and take it as the unit of energy.

The Hamiltonian of the system can be written as

$$H = H_0 + V, \quad (\text{B1})$$

with

$$\begin{aligned} H_0 &= \sum_{x\text{-link}} \sigma_i^x \sigma_j^x + \sum_{y\text{-link}} \sigma_i^y \sigma_j^y + \Lambda_2 \sum_{z\text{-link}} \sigma_i^z \sigma_j^z, \\ V &= \Lambda_1 \sum_{x'\text{-link}} \sigma_i^x \sigma_j^x + \Lambda_1 \sum_{y'\text{-link}} \sigma_i^y \sigma_j^y + \Lambda_1 \Lambda_2 \sum_{z'\text{-link}} \sigma_i^z \sigma_j^z, \end{aligned} \quad (\text{B2})$$

where V is a perturbation.

As in Ref. 3, we calculate the effective Hamiltonian as

$$\begin{aligned} H_{\text{eff}} &= \Upsilon^\dagger (V + VG'_0V + VG'_0VG'_0V + \dots) \Upsilon \\ &= H^{(1)} + H^{(2)} + H^{(3)} + \dots, \end{aligned} \quad (\text{B3})$$

where Υ maps the effective Hilbert space onto the ground-state subspace of H_0 and G'_0 is the Green function for excited states of H_0 . The ground state of H_0 is a direct-product state consisting of the ground states of the following Hamiltonians:

$$\begin{aligned} H_{p_1} &= \sigma_1^x \sigma_3^x + \sigma_2^y \sigma_3^y + \Lambda_2 \sigma_1^z \sigma_2^z, \\ H_{p_2} &= \sigma_2^x \sigma_3^x + \sigma_1^y \sigma_2^y + \Lambda_2 \sigma_1^z \sigma_3^z, \end{aligned} \quad (\text{B4})$$

defined on down-pointing and up-pointing triangles [see Fig. 1(b)].

In Eq. (B3), $H^{(1)} = \Upsilon^\dagger V \Upsilon$ is obtained as

$$H^{(1)} = \Lambda_1 \left(\sum_{x'\text{-link}} \sigma_i^x \sigma_j^x + \sum_{y'\text{-link}} \sigma_i^y \sigma_j^y + \Lambda_2 \sum_{z'\text{-link}} \sigma_i^z \sigma_j^z \right). \quad (\text{B5})$$

As in the perturbation method used for the Kitaev model on a honeycomb lattice in the presence of a weak magnetic field,³ in order to derive $H^{(2)} = \Upsilon^\dagger VG'_0V\Upsilon$, we assume that all the involved excited states of the system have a gap $\varepsilon \sim |\Lambda_2|$ above the ground-state energy. This gives rise to

$$\begin{aligned} H^{(2)} &= -\frac{MN\Lambda_1^2}{6|\Lambda_2|} (2 + \Lambda_2^2) \\ &\quad - \frac{\Lambda_1^2}{|\Lambda_2|} \left(\sum_{x'\text{-link}} \sigma_i^x \sigma_j^x \right) \left(\sum_{y'\text{-link}} \sigma_k^y \sigma_l^y \right) \\ &\quad - \frac{\Lambda_1^2 \Lambda_2}{|\Lambda_2|} \left(\sum_{x'\text{-link}} \sigma_i^x \sigma_j^x \right) \left(\sum_{z'\text{-link}} \sigma_k^z \sigma_l^z \right) \\ &\quad - \frac{\Lambda_1^2 \Lambda_2}{|\Lambda_2|} \left(\sum_{y'\text{-link}} \sigma_i^y \sigma_j^y \right) \left(\sum_{z'\text{-link}} \sigma_k^z \sigma_l^z \right). \end{aligned} \quad (\text{B6})$$

It is interesting to note that though $H^{(2)}$ involves even number of spin operators, it is not invariant under a time reversal transformation in the uniform-flux sector. Take one sum in the second line of Eq. (B6) as an example:

$$\begin{aligned} H_p^{(2)} &= -\frac{\Lambda_1^2}{|\Lambda_2|} \sum_{\langle jk \rangle = z\text{-link}} \sigma_i^x \sigma_j^x \sigma_k^y \sigma_l^y \\ &= -\frac{\Lambda_1^2}{|\Lambda_2|} \sum_{\langle jk \rangle = z\text{-link}} (\sigma_j^x \sigma_k^y \sigma_m^z) \sigma_m^z \sigma_i^x \sigma_l^y, \end{aligned} \quad (\text{B7})$$

where (j, k, m) denotes the three sites in either a down-pointing or up-pointing triangle, which is labeled by either $(2, 1, 3)$ or $(1, 3, 2)$ in Fig. 1(b). Namely, $\sigma_j^x \sigma_k^y \sigma_m^z$ is either the plaquette operator P_1 or P_2 . Since the

eigenvalues of P_1 and P_2 are both chosen to be 1 in the uniform-flux sector, $H_p^{(2)}$ can be reduced to involve only three spin operators in this sector and the time reversal symmetry is now broken. Thus, in the uniform-flux sector, one has

$$\mathcal{T} H^{(2)} \mathcal{T}^{-1} \neq H^{(2)}, \quad (\text{B8})$$

where \mathcal{T} is the time reversal transformation. Similarly, $H^{(3)} = \Upsilon^\dagger VG'_0VG'_0V\Upsilon$ can be obtained as

$$\begin{aligned} H^{(3)} &= \frac{\Lambda_1^3 (1 + \Lambda_2^2) MN}{3\Lambda_2^2} \left(\sum_{x'\text{-link}} \sigma_i^x \sigma_j^x + \sum_{y'\text{-link}} \sigma_i^y \sigma_j^y \right) \\ &\quad + \frac{2\Lambda_1^3 MN}{3\Lambda_2} \sum_{z'\text{-link}} \sigma_i^z \sigma_j^z \\ &\quad + \frac{6\Lambda_1^3}{\Lambda_2} \sum_{(i_1, i_2, i_3) \neq \Delta, \nabla} \sigma_{i_1}^x \sigma_{j_1}^x \sigma_{i_2}^y \sigma_{j_2}^y \sigma_{i_3}^z \sigma_{j_3}^z \\ &\quad + H_p^{(3)}. \end{aligned} \quad (\text{B9})$$

Here (i_1, j_1) are the two sites connected by an x' -link, (i_2, j_2) are the two sites connected by a y' -link, and (i_3, j_3) are the two sites connected by a z' -link.

$$\begin{aligned} H_p^{(3)} &= \frac{6\Lambda_1^3}{\Lambda_2} \sum_{\nabla} P_1(m, n) \sigma_{m, n-1}^y \sigma_{m, n+3}^x \sigma_{m-1, n+1}^z \\ &\quad + \frac{6\Lambda_1^3}{\Lambda_2} \sum_{\Delta} P_2(m, n) \sigma_{m, n-1}^x \sigma_{m, n+3}^y \sigma_{m+1, n+1}^z, \end{aligned} \quad (\text{B10})$$

where $\nabla(\Delta)$ runs over all down-pointing (up-pointing) triangles with (m, n) denoting the site 5 (1) in each unit cell (see Fig. 5). By summing over $H^{(1)}$, $H^{(2)}$ and $H^{(3)}$, the effective Hamiltonian, up to the third order, is given by

$$\begin{aligned} H_{\text{eff}} &= H_0^{(3)} + \frac{6\Lambda_1^3}{\Lambda_2} \sum_{\nabla} P_1(m, n) \sigma_{m, n-1}^y \sigma_{m, n+3}^x \sigma_{m-1, n+1}^z \\ &\quad + \frac{6\Lambda_1^3}{\Lambda_2} \sum_{\Delta} P_2(m, n) \sigma_{m, n-1}^x \sigma_{m, n+3}^y \sigma_{m+1, n+1}^z, \end{aligned} \quad (\text{B11})$$

where $H_0^{(3)}$ is a term involving none of the plaquette operators P_i , $i = 0, 1$ and 2.

For the QPT between two phases of the same Chern number, the parameter Λ_1 changes its sign at the transition point. This yields the change of signs in certain terms in the effective Hamiltonian. Therefore, the effective Hamiltonian H_{eff} is different at the two sides of the transition point $\Lambda_1 = 0$.

-
- ¹ S. Sachdev, *Quantum Phase Transitions* (Cambridge University Press, Cambridge, 1999).
 - ² X. G. Wen, Phys. Rev. Lett. **90**, 016803 (2003).
 - ³ A. Kitaev, Ann. Phys. (N.Y.) **321**, 2 (2006).
 - ⁴ X. Y. Feng, G. M. Zhang, and T. Xiang, Phys. Rev. Lett. **98**, 087204 (2007).
 - ⁵ H. Yao and S. A. Kivelson, Phys. Rev. Lett. **99**, 247203 (2007).
 - ⁶ S. Yang, S. J. Gu, C. P. Sun, and H. Q. Lin, Phys. Rev. A **78**, 012304 (2008).
 - ⁷ C. Nash and D. O'Connor, Phys. Rev. Lett. **102**, 147203 (2009).
 - ⁸ F. A. Bais, J. K. Slingerland, and S. M. Haaker, Phys. Rev. Lett. **102**, 220403 (2009).
 - ⁹ X. F. Shi, Y. Yu, J. Q. You, and F. Nori, Phys. Rev. B **79**, 134431 (2009).
 - ¹⁰ S. B. Chung, H. Yao, T. L. Hughes, and E. A. Kim, Phys. Rev. B **81**, 060403(R) (2010).
 - ¹¹ G. Kells, D. Mehta, J. K. Slingerland, and J. Vala, Phys. Rev. B **81**, 104429 (2010).
 - ¹² It is shown in Ref. 5 that when both J_α and J'_α are positive, the ground state is either in the uniform-flux sector or in the sector related by the time reversal transformation. Based on this, one can easily prove that this applies to the cases with arbitrary J_α and J'_α .
 - ¹³ S. Dusuel, K. P. Schmidt, J. Vidal, and R. L. Zaffino, Phys. Rev. B **78**, 125102 (2008).
 - ¹⁴ D. J. Thouless, M. Kohmoto, M. P. Nightingale, and M. den Nijs, Phys. Rev. Lett. **49**, 405 (1982).
 - ¹⁵ X. L. Qi, Y. S. Wu, and S. C. Zhang, Phys. Rev. B **74**, 045125 (2006).
 - ¹⁶ D. I. Uzunov, *Introduction to the Theory of Critical Phenomena* (World Scientific, Singapore, 1993).
 - ¹⁷ F. D. M. Haldane, Phys. Rev. Lett. **61**, 2015 (1988).
 - ¹⁸ E. Lieb, T. Schultz, and D. Mattis, Ann. Phys. (N.Y.) **16**, 407 (1961).